Three-Tether Axisymmetric Wave Energy Converter: Estimation of Energy Delivery

Nataliia Y. Sergiienko*, Benjamin S. Cazzolato†, Boyin Ding‡ and Maziar Arjomandi§
*School of Mechanical Engineering
University of Adelaide, Adelaide, South Australia, 5005 Australia
nataliia.sergiienko@adelaide.edu.au
†benjamin.cazzolato@adelaide.edu.au
‡boyin.ding@adelaide.edu.au
§maziar.arjomandi@adelaide.edu.au

***Abstract*—There are numerous designs and concepts that have been offered to extract energy from ocean waves. A heaving buoy is distinguished as the most popular prototype which predominantly harnesses energy from the vertical motion in waves. In contrast to such devices, a three-tether wave energy converter (WEC) utilises heave, surge and pitch motion modes to increase the total power absorption of the system. The current paper investigates the performance of the three-tether WEC under irregular wave conditions considering various criteria, such as the annual mean power, characteristic mass, wetted surface and significant power take-off (PTO) force. A comprehensive analysis of buoys with different shapes, aspect ratios and masses is included in this study. Thus, the trade-off between different cost-related performance measures gives a clear comparison of this WEC against other existing prototypes.**

***Index Terms*—Wave energy converter, axisymmetric point absorber, linear time domain model, energy delivery.**

I. Introduction

Intensive research on extracting energy from ocean waves started in 1970s leading to a large number of WEC units with various working principles. However, despite a wide range of WECs technologies on offer, none of the existing prototypes has reached the mass production stage still remaining at the proof-of-concept development phase. Therefore, researchers and engineers continue to offer new designs and technologies in order to make wave power conversion more competitive relative to other sources of renewable energy. One such idea is the submerged point absorber which is connected to three cables in order to control more degrees of freedom (heave, surge and pitch) as compared to the conventional heaving buoy. Consequently, this allows the absorption of more power from one WEC unit for the same buoyant actuator.

The concept of the three-tether WEC (see Fig. 1) was introduced in [1], where the system under consideration consists of a submerged spherical buoy, three tethers that are equally distributed around the buoy and each tether is connected to the individual power take-off mechanism at the sea floor. Later, the three-tether converter with a floating cylindrical buoy was used as a prototype for the control system design in [2], [3]. Further analysis has been focused more on the design features of the three-tether WEC trying to identify an optimal arrangement of tethers that will provide the maximum power output of the converter [4]. In addition, there is interest in developing wave energy arrays consisting of multi-tether buoys [5], [6]. However, the power absorption potential of this WEC type has not been estimated in realistic wave conditions and cannot be compared against other prototypes.

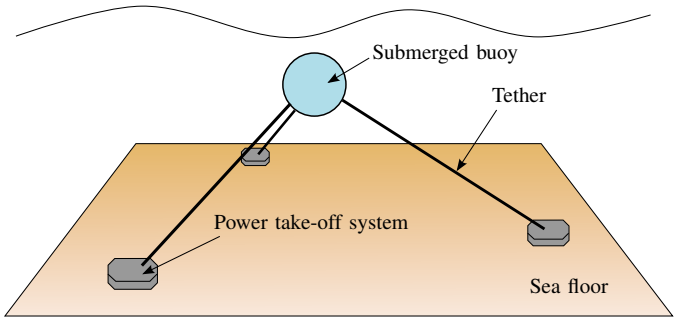

Fig. 1: Schematic representation of a three-tether WEC (adapted from [7]).

As a result, the current paper is the first attempt to understand the behaviour of the three-tether WEC in irregular wave conditions. Converters of different shapes, aspect ratios and masses are used in this study in order to identify their influence on the range of performance measures. Finally, the results are presented as a comparison between one-tether and multi-tether power take-off arrangements.

II. System parameters

Currently there is no existing prototype of the three-tether WEC which could be used in the present study. Therefore, the starting point would be to choose the expected location of the operational sea site and identify an appropriate size of the buoy. Thus, the site on the east coast of Australia has been selected for this analysis (see Table I and Figure 2 for the wave data and location).

A. Buoy size and shape

According to the methodology presented in [9], the volume of the WEC should be chosen to guarantee the maximum efficiency of the system at least one-third of the year. For the chosen NSW site the most common sea states have a

TABLE I: Australia/New South Wales (NSW) test site.

Location:	34°00'00.0"S, 152°30'00.0"E
Water depth:	deep water
Mean wave power:	23.2 kW/m (Pierson-Moskowitz)
Type of data:	hindcast (Australian Wave Energy Atlas) [8]

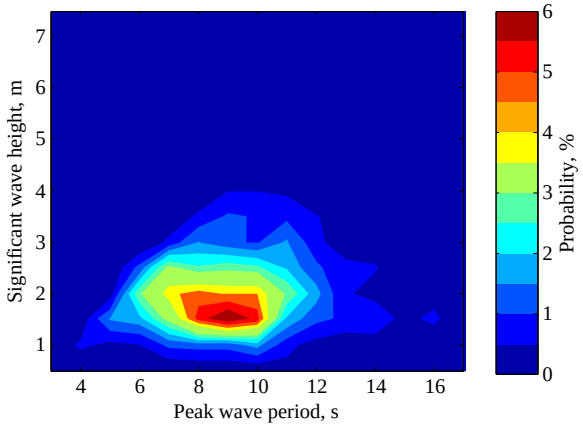

Fig. 2: Wave data statistics for NSW sea site detailed in Table I.

significant wave height of $H_s = 1.5{-}2$ m, peak wave period of $T_p = 8{-}10$ sec, and the wave power level exceeds 19.6 kW/m about one-third of the year which corresponds to the power in a regular wave of $T \approx 8$ sec and $H \approx 1.6$ m [10]. In contrast to the floating converters, an optimal volume of the submerged buoy depends not only on the wave conditions, but also on the body shape, submergence depth and volume stroke [11]. Thus, a spherical converter of $a = 5$ m radius with its centre placed $1.75a = 8.75$ m below the mean water level will absorb the maximum power at the regular wave of $T = 8$ sec and $H = 1.6$ m. The geometric parameters of the spherical buoy investigated in this study are listed in Table IV.

TABLE II: Parameters of the benchmark WEC.

Parameter	Value	Unit
Shape	sphere	
Radius	5	m
Water depth	50	m
Submersion (top of the buoy)	3.75	m
Submergence depth (centre of the buoy)	8.75	m
Volume	524	m^3
Stroke length	6 ($\pm$3)	m

To conduct a more comprehensive analysis of the 3-tether WECs, other body shapes are investigated keeping the same: (i) volume of 524 m^3, (ii) distance from the top of the buoy to the water surface of 3.75 m, and (iii) the maximum tether stroke of 3 m. As a result, four cylindrical buoys with different aspect ratios have been added to the investigation (see Table III). All geometries used in this paper are shown on Fig. 3.

Other important parameters of the WEC, such as the mass of the buoy and the inclination angle of tethers will be kept as variables throughout this paper.

TABLE III: Parameters of the cylindrical WECs with various aspect ratios.

		Height to radius ratio h_c/a			
Parameter	Unit	0.5	1	2	3
Radius, a	m	6.93	5.50	4.37	3.82
Height, h_c	m	3.47	5.50	8.74	11.45
Submergence depth (centre of the buoy)	m	5.48	6.50	8.12	9.47
Volume, V	m^3		524		

B. Power take-off

For the current study it is assumed that each tether is connected to an individual power take-off mechanism which can be implemented as an electric generator [2] or a hydraulic circuit [12]. The load force exerted on the buoy from each PTO system is presumed to have linear spring and damper effects being proportional to the tether extension and the rate of change of the tether extension.

III. Equation of Motion

The wave-to-wire model is based on the linear wave theory assuming small motion amplitudes of the buoy as compared to the length of the mooring lines (tethers). The only second order hydrodynamic effect included in the model is a viscous drag force which is proportional to the square of the body velocity relative to the fluid.

A. Kinematics

A schematic of a three-tether WEC is shown on Figure 4. The spatial arrangement of all tethers is defined by $\mathbf{s}_i$:

$$\mathbf{s}_i = \mathbf{r} + \mathbf{R}\mathbf{n}_i - \mathbf{d}_i, \quad i = 1 \dots 3, \tag{1}$$

where $\mathbf{r}$ is the position vector of a buoy in the reference coordinate frame $Oxyz$, $\mathbf{R}$ is a rotation matrix of the buoy with respect to the reference frame, $\mathbf{n}_i$ denotes the position vector of the anchor point of the i-th tether on the hull relative to the buoy centre of mass G, $\mathbf{d}_i$ is the position vector of the anchor point of the i-th tether on the sea floor in the $Oxyz$ coordinate frame. The instantaneous tether length is:

$$l_i = \|\mathbf{s}_i\| = \sqrt{\mathbf{s}_i^\intercal \mathbf{s}_i}, \quad i = 1 \dots 3, \tag{2}$$

and the change in the tether length is $\Delta l_i = l_i - l_0$.

Mapping from the buoy velocities in a Cartesian coordinate frame to the rate of change of the tether length is provided by the inverse kinematic Jacobian:

$$\dot{\mathbf{q}} = \mathbf{J}^{-1}\dot{\mathbf{x}}, \tag{3}$$

where $\mathbf{x} = [\mathbf{r} \quad \theta]^\intercal$ is the buoy location vector with three translational and three rotational motions, $\mathbf{q} = [l_1 \quad l_2 \quad l_3]^\intercal$ is a vector of three tether length variables and an inverse kinematic Jacobian $\mathbf{J}^{-1}$ can be obtained as:

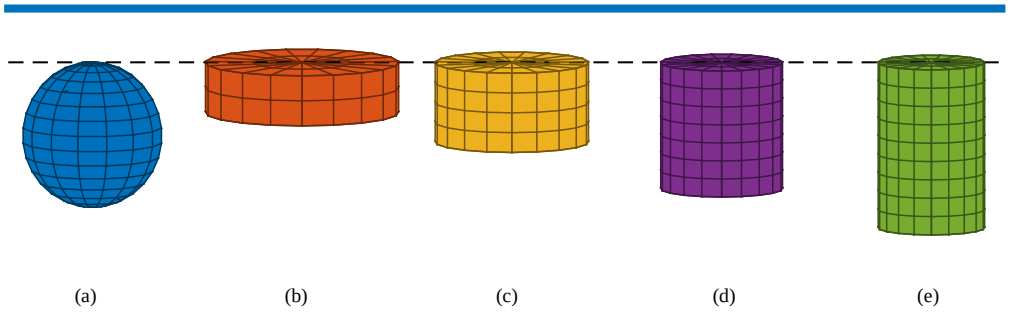

Fig. 3: Shapes of WECs: (a) sphere, (b) cylinder $h_c = 0.5a$, (c) cylinder $h_c = 1a$, (d) cylinder $h_c = 2a$, (e) cylinder $h_c = 3a$. All buoys have the same displaced volume and the same distance between their top surface and the mean water level.

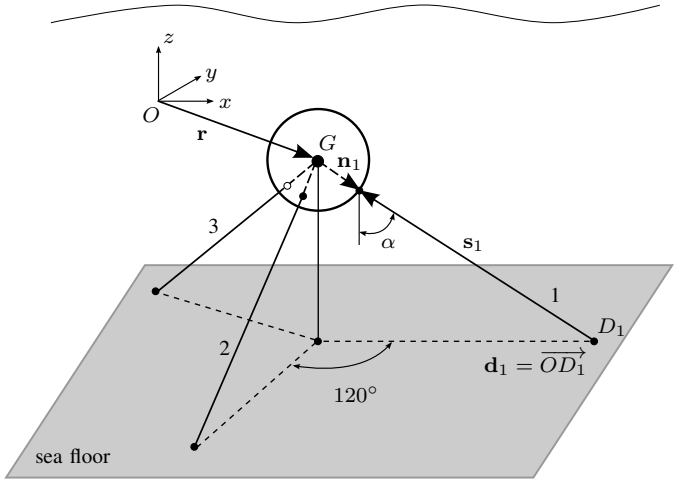

Fig. 4: Schematic of the three-tether wave energy converter.

$$\mathbf{J}^{-1} = \begin{pmatrix} \mathbf{e}_{s1}^{\intercal} & (\mathbf{R}\mathbf{n}_1 \times \mathbf{e}_{s1})^{\intercal} \\ \mathbf{e}_{s2}^{\intercal} & (\mathbf{R}\mathbf{n}_2 \times \mathbf{e}_{s2})^{\intercal} \\ \mathbf{e}_{s3}^{\intercal} & (\mathbf{R}\mathbf{n}_3 \times \mathbf{e}_{s3})^{\intercal} \end{pmatrix}, \tag{4}$$

where $\mathbf{e}_{si}$ is a unit-vector along the tether i, so $\mathbf{e}_{si} = \dfrac{\mathbf{s}_i}{\|\mathbf{s}_i\|}$.

B. Forces

The generalised forces that act on the body are expressed in the Cartesian coordinate frame $Oxyz$ as vectors of six elements including horizontal and vertical forces and rotational moments.

1) Hydrostatic force: As the buoy is fully submerged, the generalised hydrostatic force is $\mathbf{F}_{buoy} = [0 \quad 0 \quad (m_w - m_b)g \quad 0 \quad 0 \quad 0]^{\intercal}$, where $m_w = \rho V$ is the mass of the displaced water, ρ is water density, V is the displaced volume of the buoy and m_b is the mass of the WEC.

2) Power take-off forces: A behaviour of the linear PTO system is modelled as [13]:

$$F_{pto,i} = (C_{pto} - B_{pto}\Delta\dot{l}_i - K_{pto}\Delta l_i), \quad i = 1\dots3, \tag{5}$$

where K_{pto} and B_{pto} are the PTO stiffness and damping coefficients (control parameters), and

$$C_{pto} = -\frac{(m_w - m_b)g}{3\cos\alpha} \tag{6}$$

is a force that counteracts the hydrostatic force in an undisturbed position, α is the tether angle relative to the vertical.

3) Hard stop forces: As each PTO system has a limited stroke, an additional force from the hard stop mechanism is exerted on the body to constrain its motion. As a result, the hard stop system is modelled by a repulsive energy potential [13]:

$$\begin{aligned} F_{hs,i} = &- K_{hs,\min}(\Delta l_i - \Delta l_{\min})u(\Delta l_{\min} - \Delta l_i) \\ &- K_{hs,\max}(\Delta l_i - \Delta l_{\max})u(\Delta l_i - \Delta l_{\max}), \end{aligned} \tag{7}$$

$i = 1\dots3$, $u(\cdot)$ is Heaviside step function, $K_{hs,\min}$ and $K_{hs,\max}$ are the hard stop spring coefficients, $\Delta l_{\min}$ and $\Delta l_{\max}$ are the stroke limits relatively to the nominal position.

4) Tension in tether: A linear superposition of the PTO and hard stop forces governs the tension in each tether. In addition, the tethers should be always under tension in order to transmit forces from the machinery:

$$F_{t,i} = \min(0, F_{pto,i} + F_{hs,i}), \quad i = 1\dots3. \tag{8}$$

$F_{pto,i}$, $F_{hs,i}$ and $F_{t,i}$ are the forces that act along the mooring line, therefore the generalised tether force in the Cartesian coordinate frame is:

$$\mathbf{F}_{tens} = \mathbf{J}^{-\intercal}\mathbf{F}_t, \tag{9}$$

where $\mathbf{F}_t = [F_{t,1} \quad F_{t,2} \quad F_{t,3}]^{\intercal}$ and $\mathbf{J}^{-\intercal}$ is the transposed inverse kinematic Jacobian.

5) Viscous damping forces: The viscous damping force is modelled according to the Morison's equation [13], [14]:

$$\mathbf{F}_{visc} = \begin{pmatrix} -\frac{1}{2}\rho \mathbf{C}_d \mathbf{A}_d \|\mathbf{V}_b - \mathbf{V}_f\| (\mathbf{V}_b - \mathbf{V}_f) \\ -\frac{1}{2}\rho \mathbf{b}_Q D^4 D \|\dot{\theta}\| \dot{\theta} \end{pmatrix}, \quad (10)$$

where $\mathbf{V}_b = \dot{\mathbf{r}}$ is the buoy velocity, $\mathbf{V}_f$ is the fluid particle velocity at the position of the centre of mass of the buoy,

$$\mathbf{C}_d = \begin{pmatrix} C_x & 0 & 0 \\ 0 & C_y & 0 \\ 0 & 0 & C_z \end{pmatrix}, \quad \mathbf{A}_d = \begin{pmatrix} A_x & 0 & 0 \\ 0 & A_y & 0 \\ 0 & 0 & A_z \end{pmatrix} \quad (11)$$

are matrices of drag coefficients and the cross-section areas of the buoy perpendicular to the direction of motion respectively,

$$\mathbf{b}_Q = \begin{pmatrix} b_{yz} & 0 & 0 \\ 0 & b_{xz} & 0 \\ 0 & 0 & b_{xy} \end{pmatrix} \quad (12)$$

is the matrix of quadratic angular damping coefficients and D is the buoy diameter.

C. Time-domain model

The buoy motion in time domain can be described using the Cummins equation that include the wave excitation and radiation forces, and other forces specified in Section III-B:

$$(\mathbf{M} + \mathbf{A}_\infty)\ddot{\mathbf{x}} = \mathbf{F}_{exc} - \int_0^t \mathbf{K}_{rad}(t-\tau)\dot{\mathbf{x}}(\tau)d\tau + \mathbf{F}_{buoy} + \mathbf{F}_{visc} + \mathbf{F}_{tens} \quad (13)$$

where $\mathbf{M}$ is a mass matrix, $\mathbf{A}_\infty$ is the matrix with infinite-frequency added mass coefficients, $\mathbf{F}_{exc}$ is the generalised wave excitation force, and $\mathbf{K}_{rad}(t)$ is a retardation function.

D. Power absorption

The energy can be generated by the PTO machinery only when the tether, attached to it, is under tension. As a result, the total instantaneous power absorbed by the WEC is calculated as:

$$P_\Sigma(t) = \sum_{i=1}^{3} P_i(t) = B_{pto} \sum_{i=1}^{3} \left(\Delta \dot{l}_i(t)\right)^2 \quad \text{if} \quad F_{t,i} < 0. \quad (14)$$

IV. Cost-related criteria for analysis

The relative capture width (RCW) is one of the most commonly used criterion for the comparison of different wave energy converters. However, this measure is not sufficient to predict whether the WEC would be economically viable and attractive for investors. Moreover, it is hard to give a precise estimation of the WEC cost due to the limited number of full-scale prototypes. Therefore, several indirect cost-related indices have been instead suggested [15] for the analysis of a traditional measure called Levelised Cost of Electricity.

As a result, the cost-related performance measures used in this study are [15]:

(i) Annual energy output per characteristic mass E_y/m_Σ;

TABLE IV: WEC performance indices.

Parameter	Notation	Comment
Mass of the buoy	m_b	The mass of the buoy hull.
Characteristic mass	m_Σ	The total mass of the buoy and foundation calculated as $m_\Sigma = m_b + 1.5(m_w - m_b)$, where 1.5 is a safety factor.
Wetted surface	A_{wet}	The surface area of the buoy hull.
Wave power	J	
Mean absorbed power	P	
Capture width ratio		$P/(2aJ)$.
Annual energy output	E_y	$E_y = 8760P$, 8760 hours per year.
Significant PTO force	F_{pto}^{RMS}	RMS value of the PTO force including initial pre-tension force.
Tether slackness		The number of times when the tether experienced slackness over one cycle (time equal to the significant wave period T_p).

(ii) Annual energy output per characteristic surface area E_y/A_{wet};

(iii) Annual energy output per significant PTO force E_y/F_{pto}^{RMS}.

V. Implementation

Hydrodynamic coefficients of all bodies in frequency domain have been obtained using analytical solutions for the sphere [16] and for cylinders [17] and validated against WAMIT [18].

In order to conduct the time domain simulations, Equation (13) has been implemented in Simulink/MATLAB with a time step of 0.01 seconds using the ode45 solver. The duration of all simulation runs has been set to $300 \times T_p$ but not less than 1200 seconds and the first $15 \times T_p$ have not been included in the analysis due to the possible transient state. The convolution integral in Equation (13) has been replaced by the state-space model using the Marine System Simulator toolbox [19]. The irregular wave time-series have been implemented using the Pierson-Moskowitz wave spectrum over the grid of significant wave heights of $H_s = 0.5 - 7.5$ m and peak wave periods $T_p = 3 - 17$ sec.

Each body geometry has been analysed using a range of tether angles from 30° to 60° with 1° increment and a range of masses from $0.15m_w$ to $0.85m_w$ (0.15, 0.3, 0.5, 0.7, 0.85). Drag coefficients used in this study have been taken from [20] and are listed in Table V.

TABLE V: Drag coefficients.

		Cylinder			
Parameter	Sphere	$h_c = 0.5a$	$h_c = 1a$	$h_c = 2a$	$h_c = 3a$
C_x, C_y	0.5	1	1	1	1
C_z	0.5	1.2	1.1	0.9	0.85
b_{xz}, b_{yz}	0	0.2	0.2	0.2	0.2

The hard stop spring coefficient is set to $K_{hs,min} = K_{hs,max} = 10^8$ N/m and the PTO control parameters K_{pto}, B_{pto} are optimised for each sea state using Simulink Design Optimization toolbox.

VI. Results

Due to the large number of parametric studies undertaken here, results that are similar for all body shapes will be demonstrated by the example of the spherical buoy only.

A. Power matrix

The performance of the 3-tether spherical WEC with the mass of $m_b = 0.5m_w$ and the initial tether angle $\alpha = 55^\circ$ is shown on Fig. 5. The average power output at the dominant sea state ($H_s = 1.5$ m and $T_p = 8$ sec) is around 65 kW and can reach 800 kW at the strongest sea states. As shown on Fig. 5(b), the level of instantaneous power is approximately 6–10 times higher than the mean power value meaning that the designed capacity of the PTO should be an order of magnitude higher than the mean expected energy output.

Tether 1 (see Fig. 4) is aligned with the direction of wave propagation and the PTO attached to it generates about a half of the total power output (see Fig. 5(c)). The other two PTOs convert the rest of energy with equal share due to the symmetry of the tether arrangement with respect to y-axis. Thus, depending on the wave direction statistics, the first PTO system may be designed as the most powerful of three. This tether arrangement shows only one extreme case, and according to the preliminary results in frequency domain, the total power output of the WEC is largely unaffected by wave direction relative to the spatial arrangement of mooring lines.

RMS values of the buoy motion in surge, heave and pitch are shown on Fig. 5(d) – 5(f). Significant motion amplitudes in all degrees of freedom are proportional to the significant wave height. Thus, the surge RMS is about 1/2 of the H_s, while heave RMS is 1/4 – 1/3 of H_s. Interesting, that these values are similar for all body geometries considered in this study. Noting that the RMS of the wave elevation amplitude is equal to $1/4H_s$, which is almost the same as the significant amplitude in heave. This means that the buoy motion is not governed by the maximum PTO stroke but is dependent on the wave amplitude. As a result, the maximum length of the stroke should be chosen according to the targeted sea state.

B. Effect of the tether angle

The inclination angle of tethers (α) affects the power absorption of the WEC, as do the PTO parameters, noting that unlike the control parameters which can be modified to suit sea conditions, the angle cannot be changed during the system lifetime. As a result, the performance of the spherical body has been analysed with a range of tether angles with optimal PTO settings for each sea state and each value of α. Thus, the matrix of the tether angles that correspond to maximum power is shown on Fig. 6. As a result, for stronger sea states the tether angle should be larger, meaning that more power will be absorbed from surge than heave. According to the sea site considered in this paper, the tether angle for the spherical body should be set to 55° for the maximum mean power.

The sensitivity of the mean absorbed power to the tether installation errors is shown on Fig. 7. The change of the angle by $\pm 5^\circ$ from its optimal value will cause a reduction in power by approximately 5%.

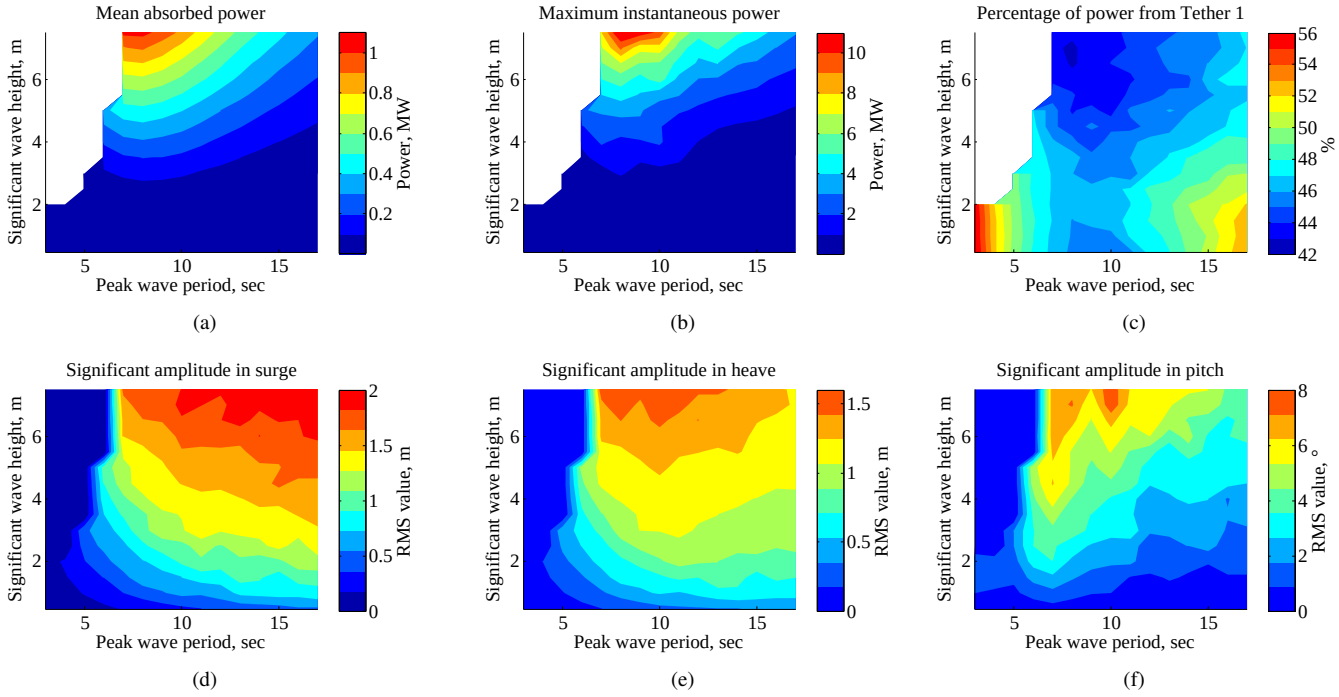

Fig. 5: Performance of the 3-tether spherical WEC. The mass of the buoy is set $m_b = 0.5m_w$, the tether angle is $\alpha = 55^\circ$, PTO parameters are optimised for each sea state.

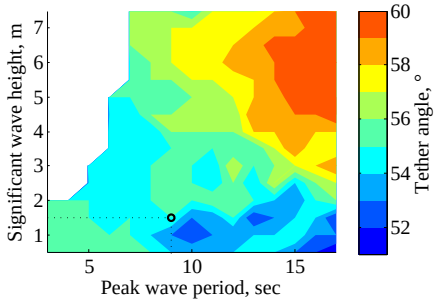

Fig. 6: Optimal tether angle of the spherical buoy with the mass of $m_b = 0.5m_w$.

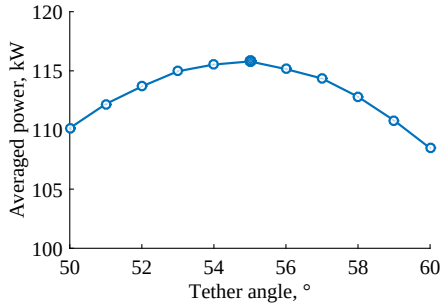

Fig. 7: The mean absorbed power of the spherical buoy at NSW site vs. the tether inclination angle. The mass of the buoy is set as $m_b = 0.5m_w$.

C. Effect of the mass

The buoy mass plays an important role in the design of the bottom-referenced WECs as it governs the weight of a foundation which in turn affects the total cost of the system. Thus, lighter buoys require larger concrete ballasts on the sea floor. However, it may be argued that the fabrication cost of the metal hull of the buoyant actuator is much higher than that of the foundation concrete and there should be a trade off between mass, capital cost and power output. As a result, the performance of the spherical buoy with a range of different masses has been investigated and the resultant cost-related criteria from Section IV are shown in Table VI. The tether angle for each mass is set such that the mean absorbed power is maximum for NSW site, PTO parameters are optimised for each sea state of each mass value.

The main conclusions that can be drawn from Table VI are:

(i) lighter buoys can produce up to 1.5 more power;
(ii) lighter buoys require the larger pretension force generated by the PTO system which may affect its cost;
(iii) the chance of slack tethers is very high for the heavy buoy of $0.85m_w$ mass;
(iv) lighter buoys more frequently hit hard stop ends (not shown here).

The performance measures from Table VI have been normalised against their maximum values and plotted on Fig. 8. Thus, for example, if the cost of the buoy is proportional to its wetted surface, if the cost of the PTO system is proportional

TABLE VI: Performance of the three-tether spherical buoy with 5 different masses.

Parameters	Unit	Mass ratio m_b/m_w 0.15	0.3	0.5	0.7	0.85
Mass of the buoy	t	81	161	268	376	456
Characteristic mass	t	765	725	671	617	577
Wetted surface	m^2			314		
Wave power	kW/m			23.2		
Mean power	kW	135	126	116	107	91
Capture width ratio	%	58	54	50	46	39
E_y/m_b	kWh/kg	14.7	6.9	3.8	2.5	1.75
E_y/m_Σ	kWh/kg	1.55	1.53	1.51	1.51	1.38
E_y/A_{wet}	MWh/m^2	3.77	3.52	3.23	3.98	2.53
E_y/F_{pto}^{RMS}	kWh/N	0.46	0.52	0.66	0.99	1.51
Tether slackness	%	4	3	2	4	30

to the force RMS and if both these values have approximately the same share in the capital cost of the WEC, then it may be concluded that the buoy mass of around $0.7m_w$ is optimal for the system. However, only WEC developers may answer the question on what mass is the most suitable for the converter from the techno-economic point of view.

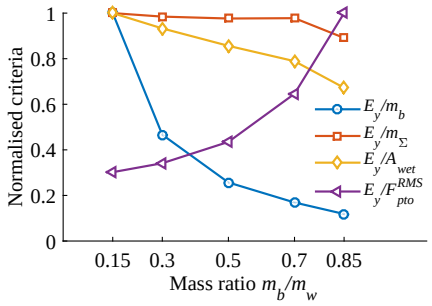

Fig. 8: Dependence of the cost-related criteria on the mass of the buoy for the 3-tether spherical converter.

D. Different shapes

In this section, the analysis of the three-tether WEC is extended to different body shapes of equal volume that are shown on Fig. 3. Also, in order to demonstrate how the multi-tether configuration is different from the generic heaving buoy connected to one tether, the same body geometries but with a one-tether PTO configuration are considered for the comparison (see Figure 9).

The submergence depth and maximum allowed tether extension are kept the same for all cases. The mass of all buoys in this section is set constant $m_b = 0.5m_w$. The time-domain model of the bottom-referenced submerged WEC with one tether has been adapted from [13]. The parameters of all WECs have been set as close as possible to each other in order to provide a fair comparison between all buoy shapes and tether configurations. However, the main discrepancy in settings refers to the constraints of the buoy motion in the Cartesian space. First of all, WECs of different shapes require different tether configurations in order to absorb maximum power as shown on Fig. 10 and explained in [4]. This property

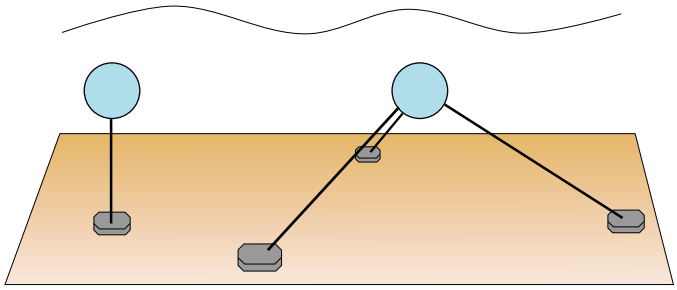

(a) (b)

Fig. 9: Different power take-off configurations for the submerged WECs: (a) the generic heaving buoy connected to one tether; (b) the three-tether system.

could be exploited by developers when optimising a site given that the spacing on the sea floor of the moorings is dependent on the optimal angle and water depth.

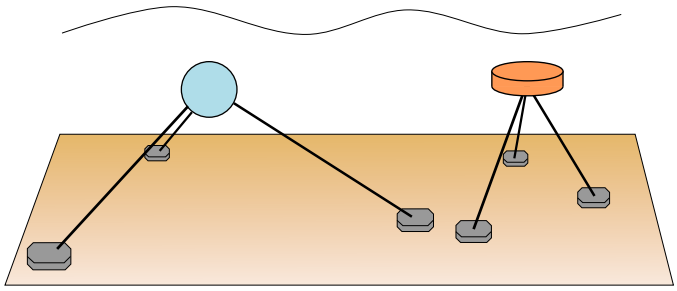

(a) (b)

Fig. 10: An example of the optimal tether configurations for different buoy shapes: (a) the spherical buoy has an optimal tether angle of $\alpha = 55°$, while (b) the flat cylinder of $h_c = 0.5a$ requires about $\alpha = 30°$.

Due to the assumption made in this study, that all converters have the same stroke length in all PTO systems, WECs of different geometries have distinctive motion envelopes depending on the tether angles which are shown on Fig. 11.

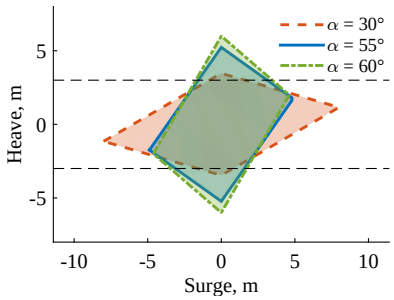

Fig. 11: A motion envelope in xz-plane of the 3-tether WEC depending on the inclination angle of tethers. The maximum stroke of each tether is 3 m. Horizontal dashed lines show motion constraints of the heaving buoy connected to one tether.

It is clear, that when tethers are closer to the vertical ($\alpha = 30°$), the converter experiences smaller motion amplitudes in heave as compared to other configurations. The corollary is that surge motion is smaller for larger tether angles. As a result, the comparison between different shapes is made keeping in mind that some of them move in heave or surge more than others and vice versa. This comment also applies to the comparison between 1-tether and 3-tether WECs. Thus, for all shapes, except the cylinder with $h_c = 0.5a$, converters with the 3-tether PTO configuration are allowed to move in heave more that their 1-tether heaving counterparts. Motion envelopes on Fig. 11 are detected from the system kinematics and only show the area where the buoy can operate without reaching hard stop mechanisms.

The resultant cost-related criteria for five WECs of different shapes calculated for NSW sea site are demonstrated on Fig. 12.

Th main outcomes from this analysis are as follows:

(i) among all 3-tether WECs, the cylinder $h_c = 0.5a$ absorbs the most power;

(ii) among all 1-tether WECs, the cylinder $h_c = 0.5a$ has the highest power output;

(iii) the 1-tether $h_c = 0.5a$ cylinder absorbs as much power as the 3-tether $h_c = 3a$ cylinder;

(iv) the 3-tether WECs can absorb 1.6 – 2.3 times more power than the same buoyant actuator connected to one tether;

(v) the 3-tether cylinders $h_c = 2a$ and $3a$ have the highest capture width ratios;

(vi) the energy output per wetted surface is the highest for the flat cylinder $h_c = 0.5a$ even though its surface area is 1.5 larger than that of the spherical body;

(vii) taller cylinders require larger inclination angles of tethers in order to absorb maximum power, which in turn require larger pre-tension forces generated in the PTO. As a result, the flat cylinder $h_c = 0.5a$ with the smallest tether angle is the most attractive from the PTO design point of view.

VII. Discussion

There are a number of uncertainties associated with the system analysis in this paper. As has been shown in [13], the power absorption results are greatly dependent on the drag coefficients taken in the model. As a result, it is necessary to assess the performance of the system using different values of viscous coefficients. Another uncertainty refers to the modelling of the PTO system which is assumed to have linear behaviour in this study. In reality, hydraulic circuits have non-linear nature which can be described by the Coulomb damping model with lower power output. Also, advanced control strategies applied to WECs may improve the mean absorbed power up to 4–5 times [9].

VIII. Conclusion

The performance of the three-tether WEC has been analysed in irregular waves using the state-of-the-art methods. It has been shown that the buoy mass reduction may lead to the

increased power output while requiring more costly PTO system and foundation. The disk-like shape of the buoyant actuator shows the best performance in terms of different cost-related measures including the mean absorbed power, the energy on wetted surface ratio and the energy on the significant PTO force ratio for both one- and multi-tether arrangements. In addition, results demonstrated that the three-tether PTO configuration can provide up to 2.3 times more power as compared to the the same buoy connected to one tether.

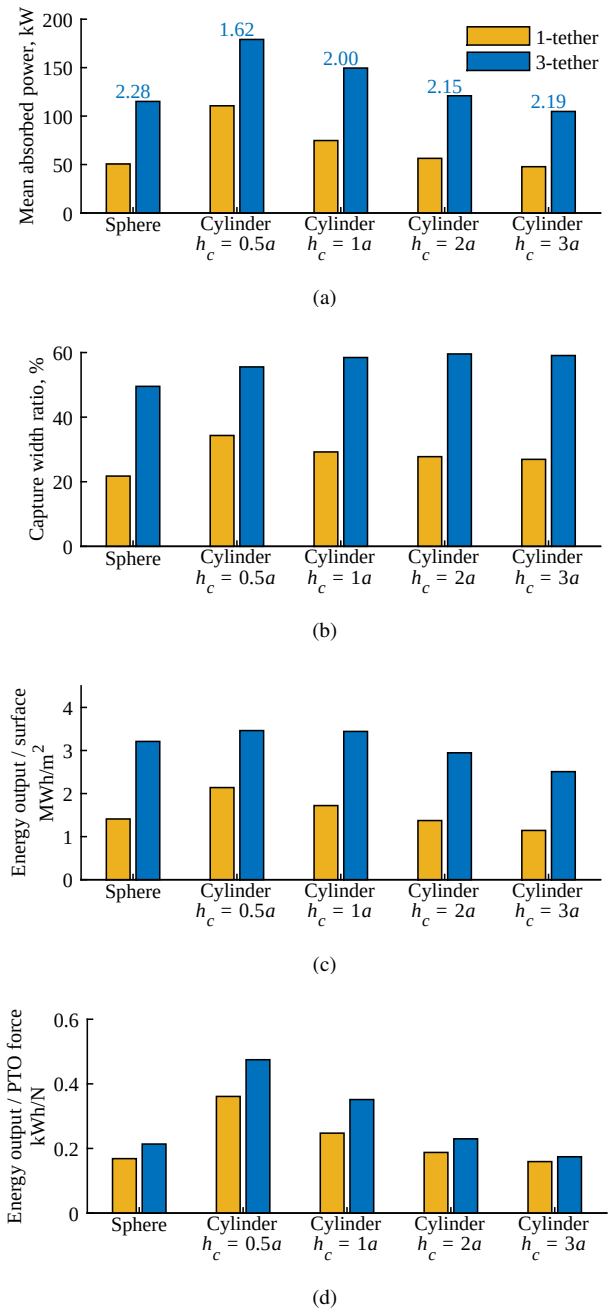

Fig. 12: Cost-related performance measures for five buoy shapes connected to one and three tethers. The annual energy output per significant PTO force for the three-tether WECs is calculated based on the PTO connected to tether 1. Values on the top of each bar on (a) show the ratio between power levels of the three-tether and one-tether units with the same buoyant actuator.

REFERENCES

[1] M. A. Srokosz, "The submerged sphere as an absorber of wave power," *Journal of Fluid Mechanics*, vol. 95, no. 4, pp. 717–741, 1979.

[2] J. T. Scruggs, S. M. Lattanzio, A. A. Taflanidis, and I. L. Cassidy, "Optimal causal control of a wave energy converter in a random sea," *Applied Ocean Research*, vol. 42, no. 2013, pp. 1–15, 2013.

[3] S. M. Lattanzio and J. T. Scruggs, "Maximum power generation of a wave energy converter in a stochastic environment," in *Proceedings on IEEE International Conference on Control Applications (CCA), 2011*. Denver, CO: IEEE, 2011, pp. 1125–1130.

[4] N. Y. Sergiienko, B. S. Cazzolato, B. Ding, and M. Arjomandi, "An optimal arrangement of mooring lines for the three-tether submerged point-absorbing wave energy converter," *Renewable Energy*, vol. 93, pp. 27–37, 2016.

[5] J. Wu, S. Shekh, N. Sergiienko, B. Cazzolato, B. Ding, F. Neumann, and M. Wagner, "Fast and effective optimisation of arrays of submerged wave energy converters," in *Proceedings on Genetic and Evolutionary Computation Conference (GECCO-2016)*, 2016.

[6] D. R. Arbones, B. Ding, N. Sergiienko, and M. Wagner, "Fast and effective multi-objective optimisation of submerged wave energy converters," in *Proceedings on 14th International Conference on Parallel Problem Solving from Nature (PPSN)*, 2016.

[7] A. Chertok, "Wave-actuated power take-off device for electricity generation," Resolute Marine Energy, Report, 2013.

[8] Australian Wave Energy Atlas, 2016, accessed 07 June 2016. [Online]. Available: http://awavea.csiro.au/

[9] J. Falnes and J. Hals, "Heaving buoys, point absorbers and arrays," *Philosophical Transactions of the Royal Society A: Mathematical, Physical and Engineering Sciences*, vol. 370, no. 1959, pp. 246–277, 2012.

[10] J. Falnes, *Ocean waves and oscillating systems: Linear interactions including wave-energy extraction*. Cambridge University Press, 2002.

[11] J. H. Todalshaug, "Practical limits to the power that can be captured from ocean waves by oscillating bodies," *International Journal of Marine Energy*, vol. 3-4, no. 2013, pp. e70–e81, 2013.

[12] Carnegie Wave Energy Limited, "What is CETO?" n.d., accessed 15 January 2015. [Online]. Available: http://www.carnegiewave.com/ceto-technology/what-is-ceto.html

[13] A. Babarit, J. Hals, M. Muliawan, A. Kurniawan, T. Moan, and J. Krokstad, "Numerical estimation of energy delivery from a selection of wave energy converters – final report," Ecole Centrale de Nantes & Norges Teknisk-Naturvitenskapelige Universitet, Report, 2011.

[14] J. Morison, J. Johnson, and S. Schaaf, "The force exerted by surface waves on piles," *Journal of Petroleum Technology*, vol. 2, no. 05, pp. 149–154, 1950.

[15] A. Babarit, J. Hals, M. Muliawan, A. Kurniawan, T. Moan, and J. Krokstad, "Numerical benchmarking study of a selection of wave energy converters," *Renewable Energy*, vol. 41, pp. 44–63, 2012.

[16] C. M. Linton, "Radiation and diffraction of water waves by a submerged sphere in finite depth," *Ocean Engineering*, vol. 18, no. 12, pp. 61–74, 1991.

[17] S. Jiang, Y. Gou, B. Teng, and D. Ning, "Analytical solution of a wave diffraction problem on a submerged cylinder," *Journal of Engineering Mechanics*, vol. 140, no. 1, pp. 225–232, 2014.

[18] C.-H. Lee, "Wamit theory manual," 1995.

[19] T. Perez and T. I. Fossen, "A Matlab toolbox for parametric identification of radiation-force models of ships and offshore structures," *Modeling, Identification and Control*, vol. 30, no. 1, p. 1, 2009.

[20] S. Hoerner, *Fluid-dynamic drag: Practical information on aerodynamic drag and hydrodynamic resistance*. Hoerner Fluid Dynamics, 1965.